Wavelet Keyhole Method: An Application of Wavelet Transform in Dynamic MRI

Wen L. Hwang and Hong N. Yeung

Dedicated to the memory of Hong N. Yeung

Abstract

We consider the processing of dynamic keyhole MRI using the wavelet-based approach. We propsosed two wavelet-based algorithms, together with careful analysis. The first algorithm embeds the conventional keyhole method as a special case in which corresponding wavelet is the Shannon wavelet while the other algorithm was proposed for the removals of the artifacts of the first method. We demonstrate that the artifacts of our method may decay faster than those of the conventional keyhole method. Our approach is fast and easy to implement. The results of several experiments are employed to access the comparative performance of both methods on a simulated phantom and clinical image.

1 Introduction

Recently, a variety of dynamic MR techniques has been proposed to follow changes in physiologic and interventional procedures. These new techniques include Flash MRI [15], echo planar imaging [23], spiral scan [13], wavelet encoding [30][24][31], SVD encoding [33], locally focused imaging [4][5][6][32], and partial update of data in the k-space [29][19][16][25][20]. Our concern here is directed toward the very last item in this list - the partial k-space update techniques. There are two reasons for this choice: first, this technique is the easiest one to implement in commercial MR scanners; second, it can provide images with high time resolution if it is combined with other fast MRI techniques [33]. The strategy used in this technique is to acquire only the essential part of the dynamic information, i.e., the part that bears the main characteristic changes in each updated image, in the k-space while leaving the parts that are unaltered to be supplemented by post-processes. This is particularly appropriate for dynamic imaging since in such cases, knowledge of "unaltered information", or the cross-sectional anatomy of the subject in question, can be acquired prior to some triggering event such as a bolus injection of a contrast agent. The supply of such a data template is most conveniently accomplished through the acquisition of a "reference" image before triggering with full spatial resolution. The advantage of this kind of technique is its simplicity in implementation. For example, keyhole imaging schemes [29][19] have been proposed for and used in applications which examine the uptake of a contrast agent and in functional studies [12]. Because of its simplicity and adaptability to the use of conventional phase encoding and Fourier-transform reconstruction, keyhole techniques can be implemented on most commercial MR scanners.

However, keyhole MRI, particularly in dynamic imaging using conventional Fourier transform(FT) reconstruction is often plagued by the problem of truncation artifacts which degrade the imaging quality and restrict its clinical application [28][17][11]. In this article, new reconstruction algorithms are proposed to circumvent the problem caused by truncation due to the abridgment of data acquisition required by the keyhole method. In this new scheme, post-processing is performed using a technique known as wavelet transform (WT), which has been shown to be useful in medical imaging [7][1]. The most significant consequence of this differ-

ence in data manipulation is manifested in the impact on the artifacts caused by the intensity mis-match resulting from the patching up of the dynamically acquired data part and from the reference template on the resulting images. In WT, this effect will depend on the choice of wavelets. We propose two WT-based algorithms in this article. The first algorithm replaces the wavelet transform coefficients of the reference data pad with those of the acquired dynamic data. We show that the conventional FT-based keyhole method is a special case of the proposed algorithm in which corresponding wavelet is the Shannon wavelet. Our second algorithm removes the artifacts arising from the former algorithm. Both methods are fast and can be easily implemented. We demonstrate that with our algorithms, the mis-matched artifact can be confined more locally in the sense that the error may decay faster than the conventional FT procedure, where this artifact is a sinc function which appears as ringing "ghosts" in whole images.

A brief summary which explains, in mathematical terms, the meaning of the wavelet transform(WT) and multiresolution analysis is given in Sec. 2. In Sec. 3, we review the conventional keyhole method. Then, the wavelet-based keyhole algorithms are proposed. Analysis of the artifacts of both methods are given. Experimental results are also shown in this section. Finally, discussion and conclusions are given in Secs. 4 and 5.

2 Results From Wavelet Theory

We first present some results of wavelet theory required in this paper. Comprehensive treatments can be found in [22][10]. Wavelet transform of a function $f(x)$ employs the expansions of the function into basis functions of the form $\psi_{j;k}(x) = 2^{-j/2}\psi(2^{-j}x - k)$, which are the integer dilating (of 2^j) and integer translating (of $2^j k$) from a single function $\psi(x)$:

$$f(x) = \sum_j \sum_k \mathcal{W}_j f(2^j k)\tilde{\psi}_{j;k}(x),$$

where

$$\mathcal{W}_j f(2^j k) = \frac{1}{2^{j/2}} \int_{-\infty}^{\infty} f(x)\overline{\psi(2^{-j}x - k)}dx.$$

The function $\psi(x)$ is called the wavelet and $\tilde{\psi}(x)$ is called the dual wavelet of $\psi(x)$. To be considered as a wavelet, $\int \psi(x)dx$ and $\int \tilde{\psi}(x)dx$ must be zero. The function $f_N(x)$ that discards the details after the scale 2^N is obtained from the partial sum with

$$f_N(x) = \sum_{j \leq N} \sum_k \mathcal{W}_j f(2^j k) \tilde{\psi}_{j;k}(x).$$

Therefore, $f(x) = f_N(x) + \sum_{j \geq N} \sum_k \mathcal{W}_j f(2^j k) \tilde{\psi}_{j;k}(x)$. The last term on the RHS of the above equation can be obtained from dilation (of 2^N) and translation (of $2^N k$) from a low-pass scaling function $\phi(x)$: $2^{-N/2}\phi(2^{-N}x - k)$. Then,

$$f(x) = f_N(x) + \sum_k \mathcal{A}_N f(2^N k) \tilde{\phi}_{N;k}(x), \tag{1}$$

where

$$\mathcal{A}_N f(2^N k) = \frac{1}{2^{N/2}} \int_{-\infty}^{\infty} f(x) \overline{\phi(2^{-N}x - k)} dx,$$

and $\tilde{\phi}(x)$ is called the dual scaling function of $\phi(x)$. Thus the Eq. (1) can be re-written as

$$f(x) = \sum_{j \leq N} \sum_k \mathcal{W}_j f(2^j k) \tilde{\psi}_{j;k}(x) + \sum_k \mathcal{A}_N f(2^N k) \tilde{\phi}_{N;k}(x).$$

Compared to Fourier transform, where the frequency resolution is precisely attained while the spatial resolution is completely lost, wavelet transform finds a compromise between these two resolutions. Hence, properties related to the local spatial frequency are preserved.

The previous construction can be extended easily to two-dimensional image using the tensor product: The low-pass scaling function in this setting is $\Phi(x, y) = \phi(x)\phi(y)$. By translating and dilating the scaling function at scale 2^j, we obtain

$$\{\Phi_{j;m,n}(x, y) = \phi_{j;m}(x)\phi_{j;n}(y) = 2^{-j}\phi(2^{-j}x - m)\phi(2^{-j}y - n) \mid m, n \in Z\}$$

There are three wavelets in this construction: $\Psi^h(x, y) = \phi(x)\psi(y)$, $\Psi^v(x, y) = \psi(x)\phi(y)$, and $\Psi^d(x, y) = \psi(x)\psi(y)$, where h,v, and d stand for the horizontal, vertical, and diagonal edges, respectively. $\Psi^h(x, y)$ detects low frequency variations along x and high frequency variations along y. Hence, it detects local horizontal edges. By the same token, $\Psi^v(x, y)$ and $\Psi^d(x, y)$ detect local vertical edges and diagonal edges, respectively.

One can easily extend Eq. (1) to its two-dimensional counterpart as:

$$\begin{aligned} f(x,y) &= \sum_{j\le N}\sum_{m,n} \mathcal{W}_j^h f(2^j m, 2^j n)\tilde{\Psi}^h_{j;m,n}(x,y) + \sum_{j\le N}\sum_{m,n} \mathcal{W}_j^v f(2^j m, 2^j n)\tilde{\Psi}^v_{j;m,n}(x,y) + \\ &\quad \sum_{j\le N}\sum_{m,n} \mathcal{W}_j^d f(2^j m, 2^j n)\tilde{\Psi}^d_{j;m,n}(x,y) + \sum_{m,n} \mathcal{A}_N^2 f(2^N m, 2^N n)\tilde{\Phi}_{N;m,n}(x,y), \end{aligned}$$

where

$$\mathcal{A}_N^2 f(2^N m, 2^N n) = \int\int f(x,y)\Phi_{N;m,n}(x,y)dxdy,$$

and

$$\mathcal{W}_j^p f(2^j m, 2^j n) = \int\int f(x,y)\Psi^p_{j;m,n}(x,y)dxdy,$$

with $p \in \{h,v,d\}$. The two-dimensional biorthogonal wavelet $\tilde{\Psi}^p(x,y)$, with $p \in \{h,v,d\}$, and scaling function $\tilde{\Phi}(x,y)$ are constructed with a tensor product from two one-dimensional biorthogonal wavelets $\tilde{\psi}(x)$, $\tilde{\psi}(y)$ and scaling functions $\tilde{\phi}(x)$, $\tilde{\phi}(y)$, respectively.

3 Method and Materials

The problem we face is how to reconstruct, given a full-resolution reference image $R(x,y)$ and a low-resolution keyhole data corresponding to a dynamic image $D_{KH}(x,y)$, an image that has a resolution equivalent to the reference and minimal artifacts. The subscript KH indicates the keyhole subspace within which the k-dynamic data is acquired. We will first review the conventional Fourier-based keyhole method. Then, we will propose our wavelet-based method. The advantage of the proposed technique will become more apparent when we analyze the two procedures in more detail in the following.

3.1 Keyhole Techniques by Means of Conventional FT Reconstruction

Let the k-space data of the reference image and the keyhole data of the dynamic images be $\hat{R}(k_x,k_y)$ and $\hat{D}_{KH}(k_x,k_y)$, respectively; the subscript KH indicates the keyhole subspace

within which the k-dynamic data is obtained. In the conventional keyhole scheme, the k-space data subjected to reconstruction is obtained by replacing the segment of the k-space data that corresponds to the key-hole subspace in the reference image $\hat{R}(k_x, k_y)$ with $\hat{D}_{KH}(k_x, k_y)$. Let

$$\hat{\theta}_{KH}(k_x, k_y) = \begin{cases} 1 & \text{if } (k_x, k_y) \text{ within } KH, \\ 0 & \text{otherwise.} \end{cases}$$

Then, the k-space data obtained using the keyhole method is given by

$$\hat{H}(k_x, k_y) = (1 - \hat{\theta}_{KH}(k_x, k_y))\hat{R}(k_x, k_y) + \hat{\theta}_{KH}(k_x, k_y)\hat{D}_{KH}(k_x, k_y).$$

The KH segment of $\hat{H}(k_x, k_y)$ is derived from the k-dynamic data and the remainder from the corresponding part of the reference data. The more conventional "zero-filled" method, which fills the data segment outside of the KH zone with zeros, can in fact be considered as a special case of the keyhole method where a zero image is used as reference. Correspondingly, a similar expression can be written in the spatial domain for the keyhole image $\hat{H}(k_x, k_y)$:

$$\begin{aligned} H(x, y) &= (\delta(x, y) - \theta_{KH}(x, y)) * R(x, y) + \theta_{KH}(x, y) * D_{KH}(x, y) \quad (2) \\ &= R(x, y) + \theta_{KH}(x, y) * (D_{KH}(x, y) - R(x, y)), \quad (3) \end{aligned}$$

where $\delta(x, y)$ is the Dirac function. In the "zero-filled" method, $R(x, y)$ is a null image and $H(x, y) = \theta_{KH}(x, y) * D_{KH}(x, y)$. The second term on the RHS of Eq. (2) thus represents the zero-filled image. Typically, in dynamic MRI, the region KH is a low-k rectangle, defined by

$$\hat{\theta}^y_{KH}(k_x, k_y) = \begin{cases} 1 & \text{if } |k_y| \leq \frac{\pi}{2p}, \\ 0 & \text{otherwise,} \end{cases}$$

where $2p$ represents the FOV of the image. The corresponding spatial counterpart of the function $\theta^y_{KH}(x, y)$ is, therefore, a sinc function of the form

$$\theta^y_{KH}(x, y) = \frac{\pi}{p}\ sinc(\frac{y\pi}{2p}).$$

The keyhole method is comparably favorable than the zero-filled method because one obtains real gain in spatial resolution by keyhole method while the zero-filled data is well known to

have the effect of pixel smoothing instead of real gain in spatial resolution. We define a distortion function $E(x,y)$, obtained by subtracting $H(x,y)$ (the reconstructed image obtained from Eq.(3)) from an ideal but hypothetical dynamic image $D(x,y)$, as:

$$\begin{aligned} E(x,y) &\equiv D(x,y) - H(x,y) \\ &= D(x,y) - R(x,y) - \theta_{KH}(x,y) * (D_{KH}(x,y) - R(x,y)) \\ &= D(x,y) - R(x,y) - \theta_{KH}(x,y) * (D_{KH}(x,y) - D(x,y) + D(x,y) - R(x,y)) \\ &= (\delta - \theta_{KH})(x,y) * (D-R)(x,y) - \theta_{KH}(x,y) * (D_{KH} - D)(x,y). \end{aligned} \tag{4}$$

Since $(D_{KH} - D)(x,y)$ contains the components of $D(x,y)$ outside of the keyhole region while $\theta_{KH}(x,y)$ is a spatial filter which retains components only in the keyhole region, the second term at the right of the equation Eq.(4) vanishes. Therefore, one obtains

$$E(x,y) = (\delta - \theta_{KH})(x,y) * (D-R)(x,y). \tag{5}$$

Eq. (5) represents the image distortion of the keyhole technique. Artifacts resulting from keyhole imaging can, thus, be understood based on Eq. (5). First, it is easy to see that $E(x,y)$ simply reflects the high spatial-frequency part of the mis-match between $D(x,y)$ and $R(x,y)$. Secondly, imaging reconstruction using the FT techniques will yield ripples centered in the region where the signal intensities of $D(x,y)$ and $R(x,y)$ are substantially different. Let us use $\theta^y_{KH}(x,y)$ as example: Let l be the keyhole size. Then, the error arising from the conventional keyhole method (FT-based keyhole) is, therefore, $(1 - l\ sinc(\frac{ly}{2})) * (D-R)(x,y)$, which has very bad spatial localization because of the slow $1/y$ decay of $sinc(ly/2)$ against y. This artifacts appear as ripples along the y direction and are mostly noticeable in places nearby the discontinuities at $(D-R)(x,y)$.

3.2 Keyhole Techniques Using Reconstruction by Means of Wavelet Transform

The alternative method we propose for the construction of keyhole images is wavelet transform (WT), or keyhole-WT in short. The major differences between this method and the keyhole-FT

scheme are the starkly different ways in these two schemes in which the dynamical image data (in the low k region) and the high-k region of the reference template are blended together. In keyhole-FT, the two data pads $\hat{D}_{KH}(k_x, k_y)$ and $(1 - \hat{\theta}_{KH}(k_x, k_y))\hat{R}(k_x, k_y)$ are simply stitched together in the k-space. In keyhole-WT, however, combination of data is accomplished in spatial or geometrical space. More precisely, the k-space data of $\hat{D}_{KH}(k_x, k_y)$ and $\hat{R}(k_x, k_y)$ are first transformed, respectively, into the spatial domain; the resultant images are then combined after performing an operation known as wavelet decomposition of the reference image, which is followed by its inverse, wavelet reconstruction. The main advantage of this approach lies in the fact that the artifacts will depend on the wavelets used in the algorithm. Actually, we will show that the conventional $\theta_{KH}(x, y)$ used in keyhole-FT can be regarded as a specially chosen wavelet, corresponding to the Shannon wavelet.

WT is an excellent tool, for the present purpose in particular, for hybridizing image data derived from different spatial frequency domains since it has the ability to preserve, in a systematic way and with different levels of resolution, the frequency characteristics of the localities in the image. To give a simply account of how WT works, it should be noted that any image can be decomposed by means of wavelet decomposition, based on its "local Fourier contents", into four sub-images, namely, LL, LH, HL, and HH, where L and H denote the low- and high-k segments of the image data, and the two-letter strings denote the combined k-characteristics of the subimage along the x and y directions, respectively. For instance, LL denotes the sub-image, which consists of low-k components in both the x and y directions, or data in the central part of the k-space in which most of the dynamic data resides. By the same token, LH stands for the sub-image, referring to its special traits in the k-space as having low k along x, and high along y, and so on for HL and HH. The sub-image LL can be further decomposed, in the same manner, into yet another four component images, each with lower resolution and a smaller number of pixels (decimated by 2 in rows and in columns). The keyhole-WT method regards the dynamically acquired image as the low resolution counterpart of a full-resolution image, the restoration of which, through supplementation of a reference, is performed in the wavelet domain. In the following, two algorithms are proposed in the embodiment of this keyhole-WT technique.

Algorithm (I)

The essence of this algorithm is that J-fold iterative wavelet decomposition is carried out on a reference image $R(x, y)$ and a dynamic image $D_{KH}(x, y)$, acquired with full resolution using the conventional keyhole method, strictly for the purpose of providing a good approximation of the full resolution dynamic image for evaluation of the algorithm. The resulting hybrid image $H(x, y)$ is obtained through wavelet reconstruction of an image formed by replacing the LL sub-image of the J-fold decomposed image of the reference image $R(x, y)$ with the corresponding sub-image $D_{KH}(x, y)$ after a series of similarly iterative decompositions. The LL part after J-fold iteration yields a keyhole 2^J times smaller in size than the fully resolved image. The smaller the keyhole size, the larger the gain in the temporal resolution and, correspondingly, larger and more numerous the artifacts in the restored image. Our algorithm is given below:

1. Perform wavelet decomposition of the reference image, R, up to scale 2^J.
2. Reconstruct a conventional FT-based keyhole image, D_{KH}.
3. Perform wavelet decomposition of D_{KH} up to scale 2^J.
4. Replace the LL part (at the scale 2^J) of R with the corresponding LL part of D_{KH}.
5. Reconstruct the image by means of wavelet reconstruction.

One can see easily that if the wavelet is chosen as Shannon wavelet, whose corresponding scaling function has a k-space response:

$$\hat{\phi}(k_x, k_y) = \begin{cases} 1 & \text{if } |k_x|, |k_y| < \pi, \\ 0 & \text{otherwise.} \end{cases} \tag{6}$$

With such a wavelet, the algorithm (I) is equivalent to the conventional FT-based keyhole method. Or, the conventional keyhole method is embedded as a specail case in which corresponding wavelet is the Shannon wavelet. In Algorithm (I), we use the wavelet representation of an image whose row and column numbers are decimated by 2 after each wavelet decomposition. This is the most popular way of image wavelet transform in literature. For convenience, we will

keep this representation hereafter. However, we should remind the reader(s) that in dynamic MRI, the decimation is applied to only one direction. In spite of the decimation is applied to either one direction or to both directions, the conclusions of our methods will not be affected.

Error Analysis of the Algorithm (I)

Experimentally, the images are discretely represented by an $M \times M$ array of pixels. Therefore, for practical purposes, if we let $R(m,n)$ and $D(m,n)$; $m,\ n \in M$, be the discrete version of $R(x,y)$ and $D(x,y)$, respectively, and express $R(m,n)$ and $D(m,n)$ in terms of N ($\leq \log_2(M)$) wavelet decompositions, we obtain the following expressions:

$$\begin{aligned} R(m,n) &= \sum_{j\leq N}\sum_{k,l} \mathcal{W}_j^h R(2^j k, 2^j l)\tilde{\Psi}^h_{j;k,l}(m,n) + \sum_{j\leq N}\sum_{k,l} \mathcal{W}_j^v R(2^j k, 2^j l)\tilde{\Psi}^v_{j;k,l}(m,n) + \\ &\quad \sum_{j\leq N}\sum_{k,l} \mathcal{W}_j^d R(2^j k, 2^j l)\tilde{\Psi}^d_{j;k,l}(m,n) + \sum_{k,l} \mathcal{A}_N^2 R(2^N k, 2^N l)\tilde{\Phi}_{N;k,l}(m,n), \end{aligned} \tag{7}$$

$$\begin{aligned} D(m,n) &= \sum_{j\leq N}\sum_{k,l} \mathcal{W}_j^h D(2^j k, 2^j l)\tilde{\Psi}^h_{j;k,l}(m,n) + \sum_{j\leq N}\sum_{k,l} \mathcal{W}_j^v D(2^j k, 2^j l)\tilde{\Psi}^v_{j;k,l}(m,n) + \\ &\quad \sum_{j\leq N}\sum_{k,l} \mathcal{W}_j^d D(2^j k, 2^j l)\tilde{\Psi}^d_{j;k,l}(m,n) + \sum_{k,l} \mathcal{A}_N^2 D(2^N k, 2^N l)\tilde{\Phi}_{N;k,l}(m,n) \end{aligned} \tag{8}$$

where

$$\begin{aligned} \mathcal{A}_N^2 D(2^N k, 2^N l) &= \sum_{m,n} D(m,n)\Phi_{N;m,n}(k,l), \quad \text{and} \\ \mathcal{W}_j^p D(2^j k, 2^j l) &= \sum_{m,n} D(m,n)\Psi^p_{j;m,n}(x,y). \end{aligned}$$

with $p \in \{h,v,d\}$. Similar to the above, we obtain $\mathcal{A}_N^2 R(2^N k, 2^N l)$ and $\mathcal{W}_j^p R(2^j k, 2^j l)$.

If $\mathcal{A}_N^2 D(.,.)$ were known, we would have obtained, after substituting it into the $\mathcal{A}_N^2 R(.,.)$ term in Eq. (7), a reconstructed image which is a hybrid of $R(m,n)$ and $D(m,n)$ consisting of the last term of the latter on the RHS of Eq.(8) and the first three terms of the former on the RHS of Eq.(7). The error image $e(m,n)$ obtained by subtracting the above reconstructed image from the hypothetical $D(m,n)$ will then be

$$\begin{aligned} e(m,n) &= \sum_{j\leq N}\sum_{k,l} \mathcal{W}_j^h (D-R)(2^j k, 2^j l)\tilde{\Psi}^h_{j;k,l}(m,n) + \sum_{j\leq N}\sum_{k,l} \mathcal{W}_j^v (D-R)(2^j k, 2^j l)\tilde{\Psi}^v_{j;k,l}(m,n) + \\ &\quad \sum_{j\leq N}\sum_{k,l} \mathcal{W}_j^d (D-R)(2^j k, 2^j l)\tilde{\Psi}^d_{j;k,l}(m,n). \end{aligned}$$

If the wavelet chosen for this application is a compact-support kind, then the error is confined locally within the region in which the intensity of the reference image and dynamic image vary significantly. However, the k-space data of $\mathcal{A}_N^2 D(2^N., 2^N.)$, which corresponds to the LL part of $D(m,n)$, with resolution reduction by a factor 2^N, is given by

$$\hat{D}(k_x, k_y)\hat{\Phi}(2^N\ k_x, 2^N\ k_y),$$

which is not the data acquired during dynamic imaging. What is usually acquired, in conventional dynamic MRI, is an image the same as $D(m,n)$ but with data confined only to a truncated part of the central k-space:

$$\hat{D}(k_x, k_y)\chi_{b^2(N,N)}(k_x, k_y),$$

where $b^2(N,N)$ represents a two-dimensional box in k-space, or a keyhole region, with a size of $\frac{2\pi}{2^N} \times \frac{2\pi}{2^N}$. For fixation of the above artifact, a complete analysis of the derivation of $\chi_{b^2(N,N)}(k_x, k_y)$ from $\hat{\Phi}(2^N\ k_x, 2^N\ k_y)$ is required. Instead of a thorough analysis, for simplicity, we adopt a simple procedure with $\mathcal{A}_N^2 D_{KH}(.,.)$ in place of $\mathcal{A}_N^2 D(.,.)$ in Algorithm (I).

We first obtain the hybridized keyhole image $H(m,n)$, which is given by

$$\begin{aligned} H(m,n) &= \sum_{j\le N}\sum_{k,l} \mathcal{W}_j^h R(2^j k, 2^j l)\tilde{\Psi}_{j;k,l}^h(m,n) + \sum_{j\le N}\sum_{k,l} \mathcal{W}_j^v R(2^j k, 2^j l)\tilde{\Psi}_{j;k,l}^v(m,n) + \\ &\quad \sum_{j\le N}\sum_{k,l} \mathcal{W}_j^d R(2^j k, 2^j l)\tilde{\Psi}_{j;k,l}^d(m,n) + \sum_{k,l} \mathcal{A}_N^2 D_{KH}(2^N k, 2^N l)\tilde{\Phi}_{N;k,l}(m,n). \end{aligned} \quad (9)$$

The distortion image $E(m,n)$ is obtained by subtracting $H(m,n)$ from $D(m,n)$:

$$E(m,n) = e(m,n) + \sum_{k,l} \mathcal{A}_N^2 (D - D_{KH})(2^N k, 2^N l)\tilde{\Phi}_{N;k,l}(m,n). \quad (10)$$

The distortion of the proposed algorithm results from choosing the wavelet which is a compromise between the two error terms of the above equation. If we choose Shannon wavelet, the scaling function of which has a support equivalent to the centrally located rectangle in the k-space (see Eq. (6)) , from which $(D - D_{KH})(m,n)$ is excluded, then this error term vanishes, which is equivalent to the conventional keyhole-FT method. However, ripples appear in the error term $e(m,n)$. Instead, if Haar wavelet is chosen, we have an error due to $e(m,n)$

which is confined locally, but the term $(D - D_{KH})(m,n)$ may result in a global error. The wavelet which best minimizes the distortion image is a subject for future investigation. Even for wavelets which do not result in the disappearance of the last term on the RHS of Eq. (10), the fact that the scaling function $\Phi_N(x,y)$ is concentrated mainly within the box $\chi_{b^2(N,N)}(k_x,k_y)$ means that we may still assume that by choosing an appropriate wavelet the error produced by this term is negligible. Based on this argument, we have the following approximation of the LL component of the difference of images

$$\mathcal{A}_N^2(D-R)(2^N.,2^N.) \;\approx\; \mathcal{A}_N^2(H-R)(2^N.,2^N.). \tag{11}$$

3.3 Restoration of Spatial Resolution Using the Reference Template

Resolution enhancement of keyhole images through supplementation of high spatial-frequency components from the reference is often marred, regardless of the reconstruction algorithm used, by artifacts resulting from the mis-match in the wavelet coefficients of the dynamic and reference images. The image reconstructed using Algorithm (I), for example, invariably appears distorted around the boundaries of the activation regions. To alleviate this serious consequence of the artifact, one needs to remove or at least minimize this "activation errors" resulting from the image mis-match between $D(m,n)$ and $R(m,n)$.

The keyhole problem or the reconstruction of a high-resolutional image from low-resolutional data with the help of a reference image is an ill-posed problem. The solution to such a problem is not unique. Usually, we rely on the regularization method to find a good solution which matches the best *a prior* constraints. Most of the existing methods use the regularization procedure to find a constrained solution the k-space response of which is equivalent to that of the dynamic data [2][26][27]. Following the same line, extending algorithm (I) to recover the activation image, we need to place constraints on the complete dynamic data to be reconstructed. The difference in the images of $D(m,n)$ and $R(m,n)$ assumes the following form based on our proposed model for solution of this problem:

$$D(m,n) - R(m,n) = \begin{cases} \sum_{r=1}^{p}(M_r - 1)R(m,n)\chi_{O_r}(m,n) & R(m,n) > 0, \\ D(m,n) & \text{otherwise}, \end{cases} \tag{12}$$

where $\chi_{O_r}(m,n)$ indicates locations of the r-th component and M_r is a constant over $\chi_{O_r}(m,n)$. In this model, we further assume that the changes of pixel intensity are proportional to their reference values. In other words, the intensity differences between the reference and the dynamic images are assumed to be made up of p well delineated but presumably uniform regions. This is a simple and reasonable model for many dynamic MRI applications.

Consider the projection P_V^N of the difference image $(D-R)(m,n)$ into the space spanned by the basis $\{\tilde{\Phi}_{N;k,l}(m,n)\}$:

$$P_V^N(D-R)(m,n) = \sum_{k,l} \mathcal{A}_N^2(D-R)(2^N k, 2^N l)\tilde{\Phi}_{N;k,l}(m,n),$$

where $\mathcal{A}_N^2(D-R)(2^N k, 2^N l)$ is the LL part of N-fold iterations of the difference image. The outcome of this, according to Eq.(12), can be written as the following expression:

$$P_V^N(D-R)(m,n) = \sum_{r=1}^{p}(M_r - 1)P_V^N(R\chi_{O_r})(m,n), \tag{13}$$

where $(R\chi_{O_r})(m,n)$ represents an image component resulting from confining the reference image $R(m,n)$ to the rth region; as a result, its projection is $P_V^N(R\chi_{O_r})(m,n)$. To simplify the calculation of the above equation, we can assume that both Φ and $\tilde{\Phi}$ are fast decaying functions; and we further assume that the boundaries of each activation region are preserved:

$$(M_r - 1)P_V^N(R\chi_{O_r})(m,n) \;\approx\; (M_r - 1)\chi_{O_r}(m,n)P_V^N R(m,n). \tag{14}$$

This assumption is a good approximation for the case where a pixel (m,n) is within or away from the boundaries of some activation. Since the projection involves filtering with Φ and $\tilde{\Phi}$, for pixels close to activation region's boundaries, this approximation becomes inappropriate. Thus, the approximation of the above equation depends on the relative size of an activation region compared to those of Φ and $\tilde{\Phi}$, and on the distance between the activation regions. Note that the loss of detecting the small objects by the keyhole method appears as well by the proposed wavelet method. For simplicity, the reference image $R(m,n)$ is assumed to contain no pixels with null values. Dividing Eq. (13) by the projection image of the LL component of the reference $R(m,n)$ and using Eq. (14), we obtain:

$$\frac{P_V^N(D-R)(m,n)}{P_V^N R(m,n)} \approx \sum_r (M_r - 1)\chi_{O_r}(m,n). \tag{15}$$

From Eq. (12), we obtain

$$(D-R)(m,n) \approx \frac{P_V^N(H-R)(m,n)}{P_V^N R(m,n)} R(m,n).$$

Then,

$$\begin{aligned} \mathcal{D}(m,n) &\approx (1+\frac{P_V^N(H-R)(m,n)}{P_V^N R(m,n)})R(m,n) \\ &= \frac{P_V^N H(m,n)}{P_V^N R(m,n)} R(m,n). \end{aligned} \tag{16}$$

This equation shows that the dynamic image $D(m,n)$ (with full resolution) can be approximated, using the above model, by weighting the reference image $R(m,n)$ with the function which is formed simply by the quotient of the LL projection images of the hybrid $H(m,n)$ and the reference $R(m,n)$.

3.4 Post-processing - Removal of Artifacts

The keyhole-WT images reconstructed using Algorithm (I) are, more often than not, tainted by artifacts. Another algorithm, referred to henceforth as Algorithm (II) according to Eq.(16), is therefore proposed solely for the purpose of reducing such artifacts.

Algorithm (II)

1. Apply Algorithm (I) and obtain $H(m,n)$.
2. Decompose $H(m,n)$ up to N levels; set to zero the wavelet coefficients of $\mathcal{W}_j^p H(m,n)$, where $p \in \{h,v,d\}$, and $j \in 1:N$.
3. Apply the wavelet reconstruction. We then obtain $P_V^N H(m,n)$.
4. Apply the same steps as above to the reference image R. We have $P_V^N R(m,n)$.
5. Obtain the resultant image $\mathcal{D}(m,n)$ from Eq.(16).
6. Apply a median filter to each activation region.

We employ the median filter in the last step of the algorithm to remove the artifact errors nearby the boundaries of activation regions. This corresponds to post-processing removal of the errors from the pixels whose intensity variations are not approximated properly by Eq.(14). The window size of a median filter is selected according to the size of the tainted regions.

3.5 Experiment Results

To compare the effectiveness of the WT and conventional FT techniques in processing dynamic keyhole image data, results from simulated phantom and clinical images processed using these two techniques were obtained. Haar wavelet were used throughout for the keyhole-WT method in our computations. Wavelet decompositions used in Algorithm (I) is inversely proportional to the dynamic-to-template fraction (DTF), which is a measure of the size of the keyhole data relative to the size of the reference, used in the keyhole method. For example, for a DTF of 25%, or 1/4, the corresponding decomposition number is 2. The DTF used in all the cases described below was 25%. It should be noted also that it was our practice to use the conventional method of implementing the multiresolution representation, that is to sample the wavelet coefficients of every other point at each scale. Thus, the reduction of resolution are carried out in both the row and column directions, notwithstanding the fact that this differs from the fast dynamic MRI method in which reduction occurs only in the phase-encoding direction.

Figs. 1, 2, 3, and 4 illustrate some of the basic salient features the WT method and shows how they differ from the conventional FT technique in reconstructing keyhole images on a circular phantom. These figures represent the results of using a variety of scenarios representing the hypothetical possibilities associated with the phantom images. Figs.1 and 2 show results of keyhole images reconstructed using a scenario in which the reference image intensity was four times stronger than the dynamic image while Figs. 1 and 3 show results obtained using a scenario which is exactly the opposite: the reference image was four times weaker in comparison to the reference. Fig. 2 shows dynamic keyhole images corresponding to the first scenario: the top left, keyhole image was reconstructed using the WT method and Algorithm (I); the top right and middle left images were reconstructed using Algorithm (II) without, and with, median

filtering (with a window size equal to 11 pixels), respectively. One can see clearly the block effects nearby the boundaries of the reconstructed middle left circle image. The block effects, due to failure to approximate the boundary pixels using Eq.(16), come from the scaling function of the Haar wavelet, which is a box function in spatial domain. The middle right reconstructed image was obtained using the conventional FT technique. The bottom left and right images are the "error" images of the respective keyhole images reconstructed using the WT(middle left image) and FT(middle right image) keyhole methods, respectively. These errors were obtained by subtracting the reconstructed image from the dynamic phantom image with full-resolution. These two error images clearly show that the WT errors tend to bundle around the activation boundary while the FT errors tend to spread by ways of ripples throughout the whole image.

Fig. 3 shows the difference in the performance of these two keyhole techniques more vividly by plotting the image intensity profile along a horizontal line drawn across the dynamic (the top and middle images) and error (the bottom left and bottom right) images. One should notice that the global error occurs in the top left plot, even with a compact supported wavelet like Haar, which is due to the mis-match of the LL part of the reference image and that of the box function. For a scenario where the intensity of the reference image becomes darker than the dynamic image, the results are shown in Fig. 4.

Fig. 5 shows the simulated results performed on a different phantom which consists of two components: one circular in shape surrounded by another square in shape. Emphasis is, once again, placed toward contrasting the comparative merit of the keyhole-WT vs. the keyhol-FT method in reconstructing the phantom's cross-sectional images under different hypothetical scenarios. One can notice from all the above experiments that the error images are not the same when the roles of the reference and the dynamic images are interchanged in both the WT-based and FT-based keyhole methods.

Finally, to appraise the practical applicability, in a clinical setting, of the keyhole-WT and its advantage, if there is any, over the more conventional keyhole-FT technique in reconstructing dynamic images, a hypothetical tumor, circular in shape with a radius about 10 pixels, or a lesion of some neurological disorder, was placed, by simulation, on the trans-axial MR tomogram of a human brain. The resulting sequence of dynamic images, with a DTF of 25%,

constructed using these two methods, depict different sequences of events in which the lesion intensity decreases chronologically, relative to the brain background. In our setting, the intensity variations of the tumor (dark area) and its neighbor increase along with the time (increasing from bottom to top). In Figs. 6 and 7, one can see from both the reconstructed and error images that the keyhole-WT method is superior to the keyhole-FT method in the case where the variation of intensity is high in a small region and the error is confined locally or decays faster than that which occurs as a result of using the conventional keyhole method.

4 Discussion

The main advantage of the keyhole-WT method over the conventional keyhole-FT technique is that the former produces images with artifacts chosen from the wavelets. Actually, the conventional keyhole-FT is a special case of the former where the corresponding wavelet is the Shannon wavelet. One can choose a wavelet such that the artifacts may be confined locally in the sense of faster decay around the boundaries of the regions having intensity variations while the latter produces more global ripple artifacts. Other advantages that the keyhole-WT method offers are: 1) There is a variety of wavelet bases that one may choose from to suit the particular need. In our experiments, the Haar wavelet was selected simply because it is the fastest one in computation and among the simplest in implementation. One drawback of the Haar basis for dynamic MRI is that it tends to produces blocky artifacts at the boundaries of activation regions. 2) The keyhole-WT algorithm as outlined above is simple to implement. Wavelet decomposition is fast and easy to compute. The wavelet codes are easy to write, and the basic package for such codes is available in many software environments. Finally, 3) Unlike previous methods where the regularization solution involves a complex inverse operation, Algorithm (II) provides a simple solution to remove the artifacts arising from Algorithm (I).

Although this new method of processing dynamic MRI has advantages over the previous approaches, there are several important issues for further research: 1) Extensive studies focusing on clinical data analysis of our keyhole approach with the conventional keyhole method should be conducted. 2) We have not implemented our method with other wavelet bases; others such

as spline wavelets are among the most interesting wavelets to try, since the spline wavelet has the minimal amount of support among all the orthogonal wavelet bases for a given smoothness. Our method could also be studied with the bi-orthogonal wavelet bases. Also, the relationship of the wavelet bases with the performance should be investigated.

5 Conclusion

A wavelet-based approach has been introduced to process images dynamic keyhole MRI. The wavelet-based approach produces artifacts chosen from wavelets. We have shown that the conventional keyhole method is a special case of our keyhole-WT method (Algorithm (I)) where the corresponding wavelet is the Shannon wavelet. Analysis of artifacts produced by the wavelet-based approach and the conventional keyhole method has shown that the former artifacts may be confined more locally in the sense of faster decay than the latter. Our approach is fast and easy to implement. The results obtained has demonstrated that wavelet-based approach is applicable to dynamic MRI application.

Acknowledge: We would like to thank Mr. Nan-Kuei Chen for his vivid discussion of the wavelet keyhole method when he worked as an assistant at Academia Sinica. Also, we thank Dr. Chen Chang at Academia Sinica for his suggestions.

References

[1] A. Aldroubi and M. Unser, "Wavelets in Medicine and Biology," *CRC,* 1996.

[2] P. Barone and G. Sebastiani, "A New Method of Magnetic Resonance Image Reconstruction with Short Acquisition Timea and Truncation Artifact Reduction," *IEEE Trans. on Medical Imaging,* Vol. 11, No. 2, 1992.

[3] N. K. Chen and H. N. Yeung, "Romoval of Gibbs Artifacts in Keyhole MRI by Iterative Wavelet Filtering," *ISMRM,* 2045, 1997.

[4] Y. Cao and D. N. Levin, "MR Imaging with Spatially Variable Resolution," *JMRI,* 1992:2:701-709.

[5] Y. Cao, D. N. Levin, "Feature Recognizing MRI," *MRM,* 30:305-317, 1993.

[6] Y. Cao, D. N. Levin, "On the Relation Bwtween Feature Recognizing MRI and MRI Encoded by Singular VAlue Decomposition," *MRM,* 33:140-142, 1995.

[7] R. Carmona, W. L. Hwang, and R. Frostig, "Wavelet Analysis of Optimal Brain Imaging," *IEEE Transaction on Medical Imaging,* vol.14, no.3, Sep. 1995, pp. 556-564.

[8] R. T. Constable and R. M. Henkelman, "Data Extrapolation for Truncation Artifact Removal," *MRM,* 17:108-118, 1991.

[9] R. T. Constable and J. Gore, "The loss of Small Objects in Variable TE Imaging: Implications for FSE, RARE, and EPI," *MRM,* 28:9-24, 1992.

[10] I. Daubechies, "Ten Lectures on wavelets," *SIAM, CBMS 61,* 1992.

[11] J. L. Durek, J. S. Lewin, and D. H. Wu, "Application of Keyhole Imaging to Interventional MRI: A Simulation Study to Predict Sequence Requirements," *JMRI,* 1996, 6, 918-924.

[12] J. H. Gao, J. Xiong, S. Lai, E. M. Haake, et. al, "Improving the temporal Resolution of Functional MR Imaging Using Keyhole Techniques," *MRM*, 6:854-860, 1996.

[13] G. H. Glover and N. Pelc, "A Rapid-Gated Cine MRI Technique," *Magn. Reson. Annu.*, 1988:299-333.

[14] C. Haupt, N. Schuff, M. Weiner, and A. Maudsley, "Removal of Lipid Artifacts in H1 Spectroscopic Imaging by Data Extrapolation," *MRM,* 35:6;78-687, 1996.

[15] A. Haase, "Snapshot FLASH MRI, application to T1, T2, and Chemicl-Shift Imaging," *MRM,* 13:77-89, 1990.

[16] X. Hu and T. Parrish, "Field of View Reduction for Dynamic Imaging," *MRM,* 31:691-694, 1994.

[17] X. Hu, "On the Keyhole Imaging," *JMRI,* 1995, 4, 2, 231.

[18] W. L. Hwang, N. K. Chen, C. Chen, and H. Yeung, "Application of Wavelet Decomposition in Dynamic MRI," *Proceedings of ISMRM,* 1996.

[19] R. A. Jones, O. Haraldseth, T. B. Muller, et al., "K-space Substitution : A Novel Dynamic Imaging Technique," *MRM,* 29:830-834, 1993.

[20] W. E. Kyriakos, L. P. Panych, G. P. Zientara, and F. A. Jolesz, "Implementation of a Reduced Field of View Method for Dynamic MR Imaging Using Navigator Echoes," *JMRI,* 1997, 7, 376-381.

[21] J. Lu, D. Healy, Jr., and J. B. Weaver, "Contrast enhancement of Medical Images using Multiscale Edge Representation," *Optical Engineering,* Vol. 33, No. 7, July 1994.

[22] S. Mallat, "A Theroy of Multiresolution Signal Decomposition: The Wavelet Representation," *IEEE Trans. PAMI,* 11(7), 1989.

[23] P. Mansfield, "Multi-Plannar Imaging Formation Using NMR Spin Echoes," *J. Phys. C: solid state phus.*, 10, L55-58, 1977.

[24] L. P. Panych and F. A. Jolesz, "A Dynamically Adaptive Imaging Algorithm for Wavelet-Encoded MRI," *MRM,* 32:738-748, 1994.

[25] T. Parrish and X. Hu, "Continuous Update with Random Encoding (cure), a New Strategy for Dynamic Imaging," *MRM,* 33:326-236, 1995.

[26] S. Plevritis and A. Macovski, "Spectral Extrapolation of Spatially Bounded Image", *IEEE trans. on Medical Imaging*, Vol. 14, No. 3, September 1995.

[27] G. Sebastiani and P. Barone, "Truncation Artifact Reduction in Magnetic Resonance Imaging by Markov Random Field Methods," *IEEE Trans. on Medical Imaging,* Vol. 14, No. 3, September 1995.

[28] T. A. Spraggins, "Simulation of Spatial and Contrast Distortions in Keyhole Imaging," *MRM* 32: 320-322, 1994.

[29] J. J. Van Vaals, M. E. Brummer, W. T. Dixon, et. al., "Keyhole method for Accelerating Imaging of Contrast Agent Uptake," *JMRI,* 3, 671-675, 1993.

[30] J. B. Weaver, Y. Xu, D. M. Healy, "Wavelet-Encoded MR Imaging," *MRM,* 24:2;75-287, 1992.

[31] M. Wendt, G. Lenz, L. Batz, et. al., "Dynamic Tracking Algorithm for Interventional MRI using Wavelet-Encoding," *Proceedings of ISMRM,* 1995: 2: 1162.

[32] L. Yao, Y. Cao, D. N. Levin, "2D Locally Focussed MRI: Applications to Dynamic and Spectroscopic Imaging," *MRM,* 1996.

[33] Gary Zientara, Lawrence Panych, Ferenc Jolesz, "Dynamically Adaptive MRI with Encoding by Singular Value Decomposition," *MRM,* 32:268-274, 1994.

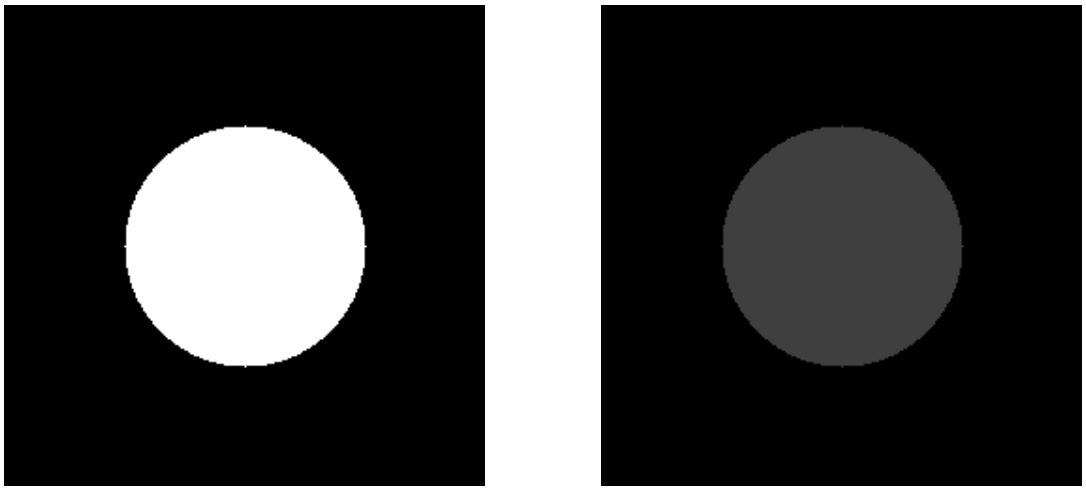

(a) (b)

Figure 1: (a). The circular phantom. (b). The circle phantom image whose intensity is four times weaker than that of the same image at (a).

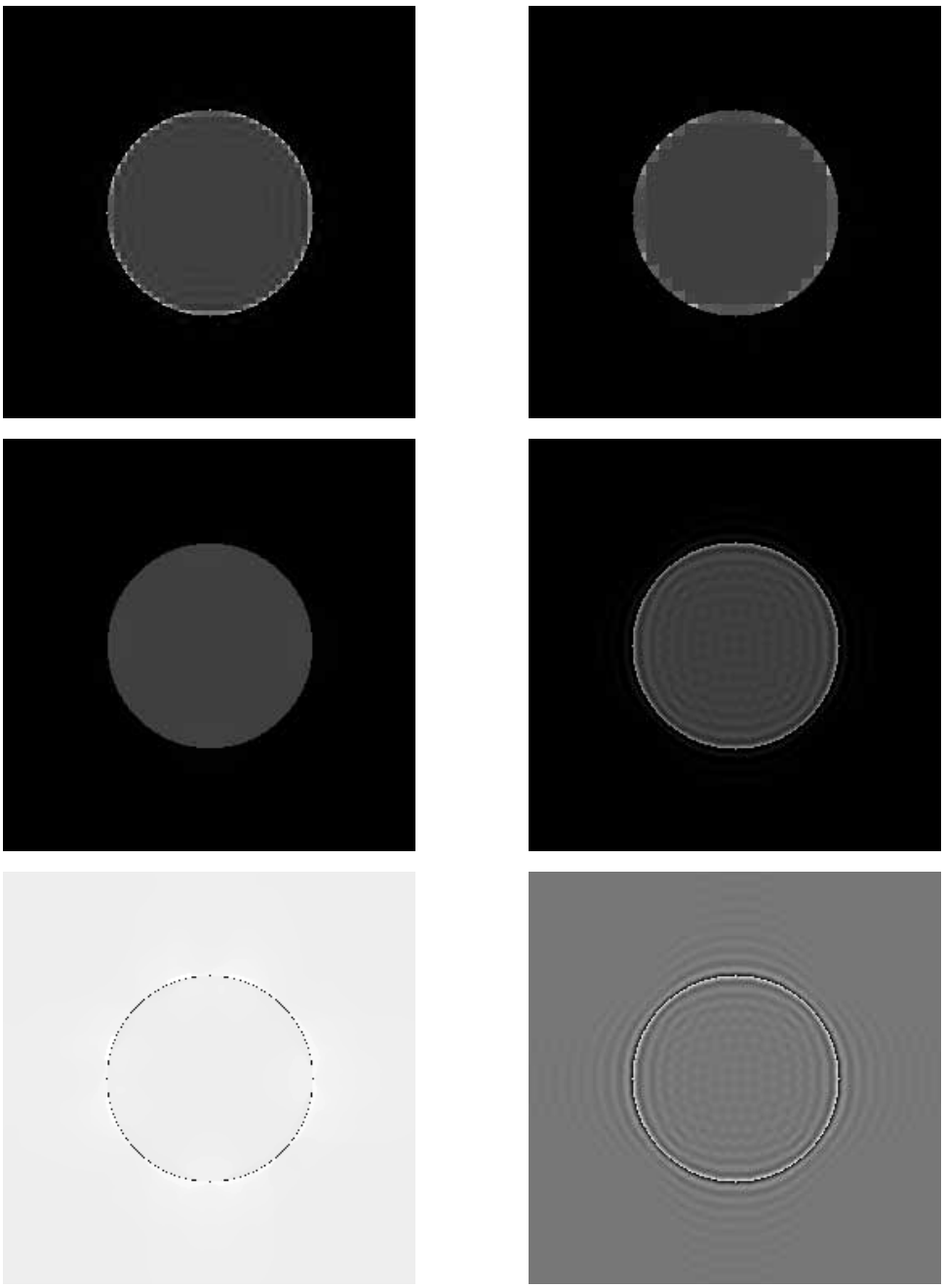

Figure 2: Top Left: Image obtained after employing Algorithm(I). Top Right: Image obtained after employing Algorithm(II) without median filtering. Middle Left: The result of processing the Top Right image using a median filter. Middle Right: The result image of using the conventional FT-based keyhole method. Bottom Left: Error image of the middle left (WT-based) image. Bottom Right: Error image of the middle right (FT-based) image.

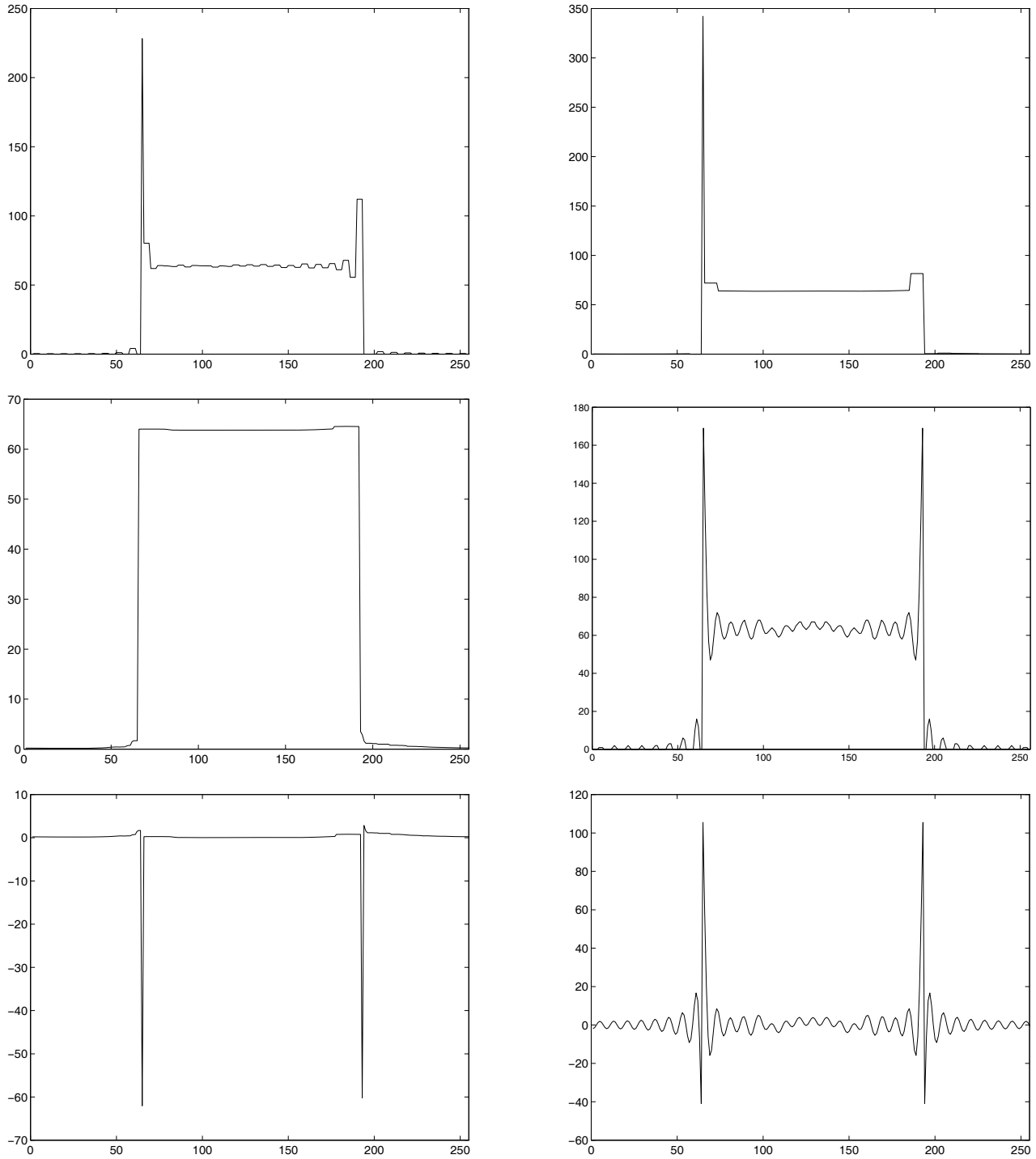

Figure 3: Image intensity profile along a middle horizontal line at Figs. in 2. Top Left: profile of the top left image. Top Right: profile of the top right image. Middle Left: profile of the middle left image. Middle Right: profile of the middle right image. Bottom Left: profile of the bottom left image. Bottom Right: profile of the bottom right image.

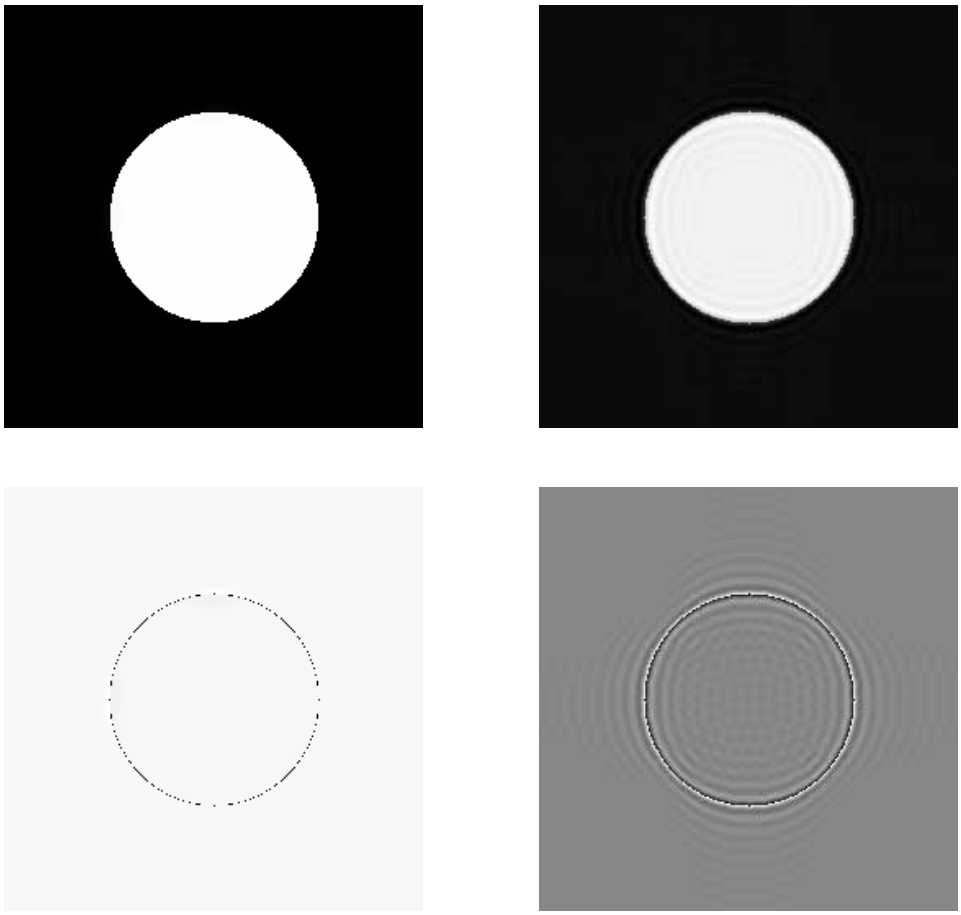

Figure 4: Reversing the role of the reference and dynamic images shown in Fig. 2; Fig. 1(b) is the reference, and Fig. 1(a) is the dynamic image. Left Top: Image reconstructed using the WT-based keyhole method. Right Top: Image reconstructed using the FT-based keyhole method. Bottom Right: Error image of the WT-based keyhole method. Bottom Left: Error image of the FT-based keyhole method.

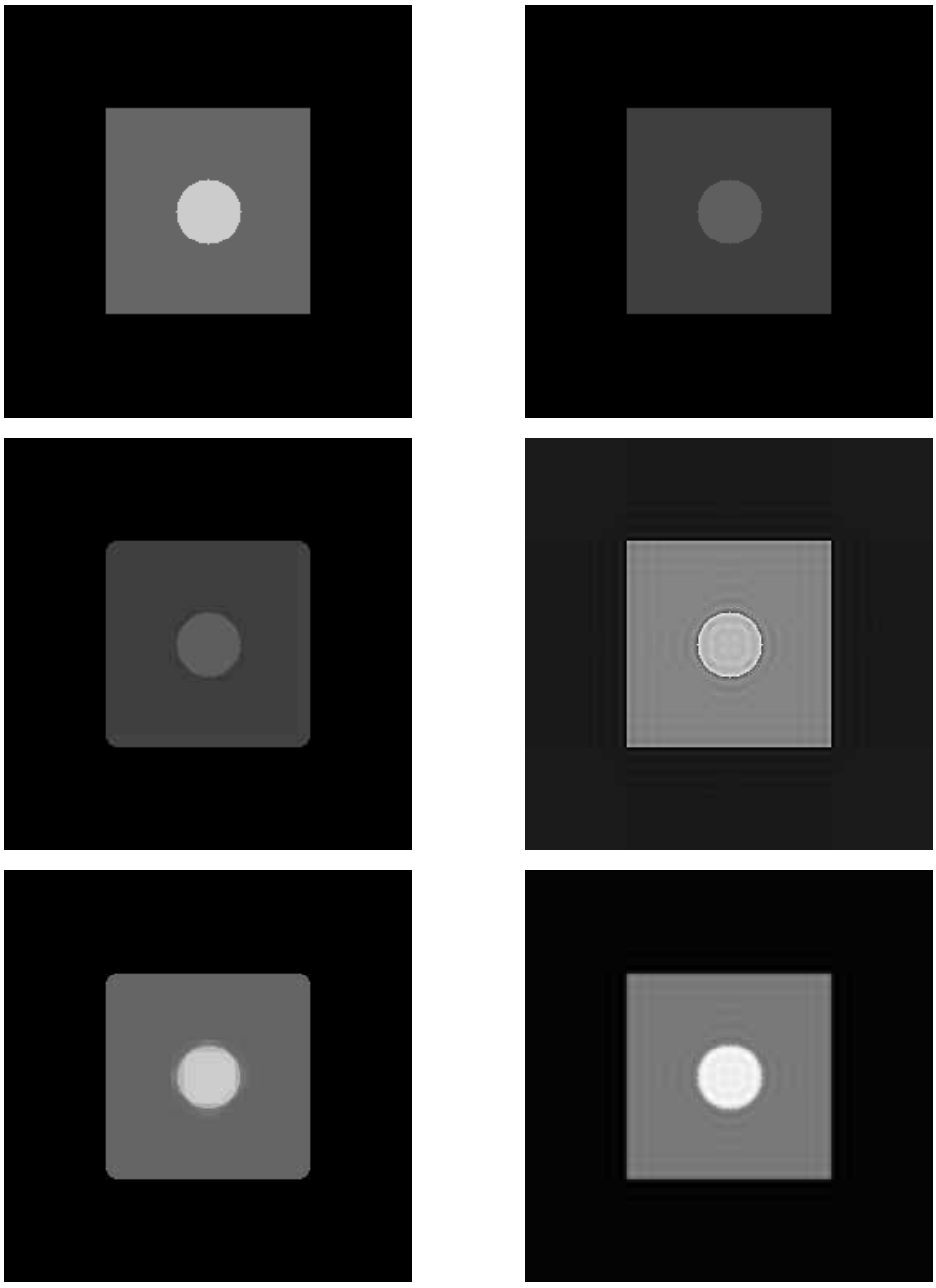

Figure 5: Top: Image with two components. Middle: Images reconstructed using the WT(Left) and FT(Right) methods, respectively. The target dynamic image is the top right image. Bottom: Images reconstructed using the WT(Left) and FT(Right) methods, respectively. The target image is at top left.

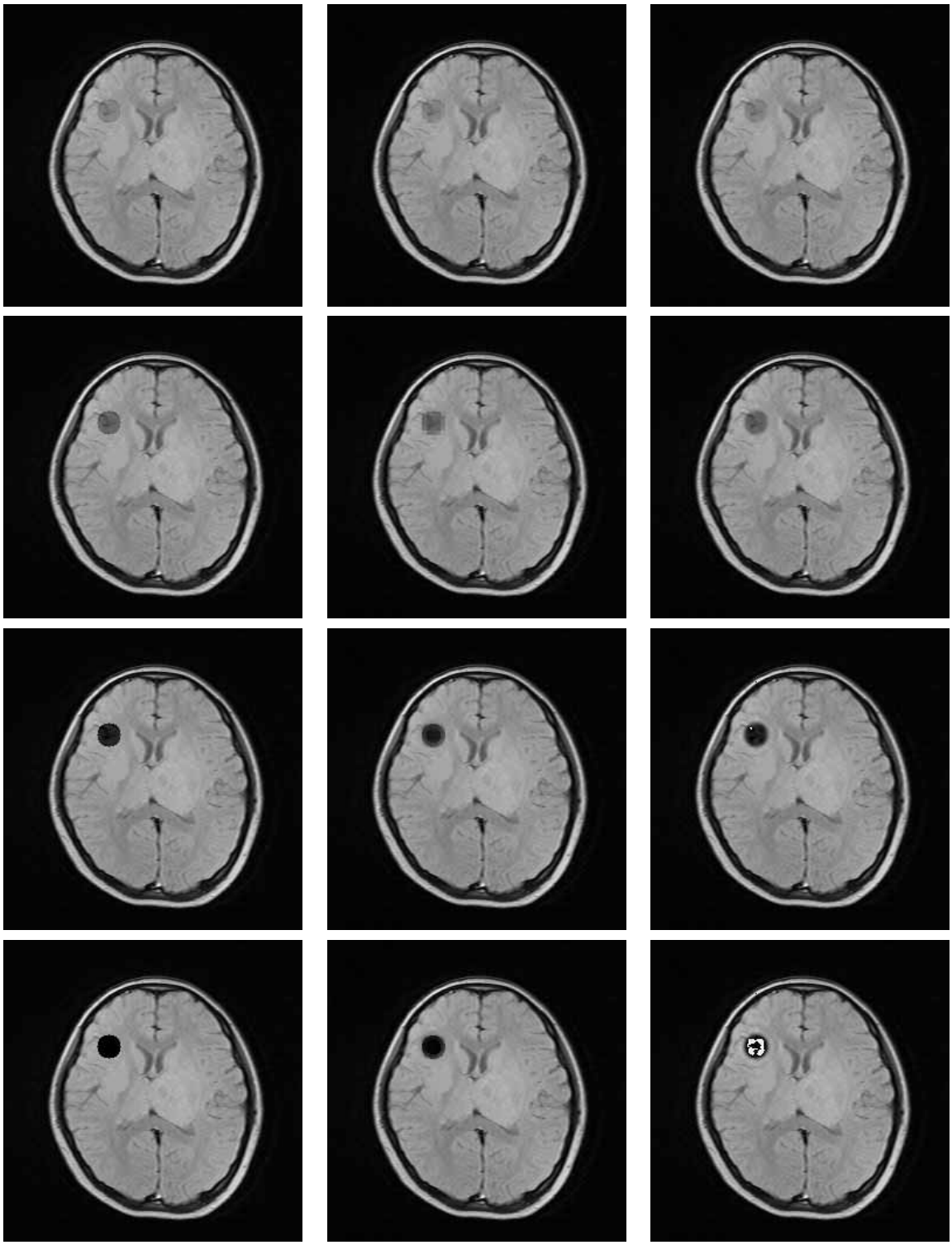

Figure 6: Left Column: Clinical dynamic sequence. DTF is 25%. Middle Column: Results of the WT-based method. Right Column: Results of the FT-based method. Notice the large error in the bottom image in the right column.

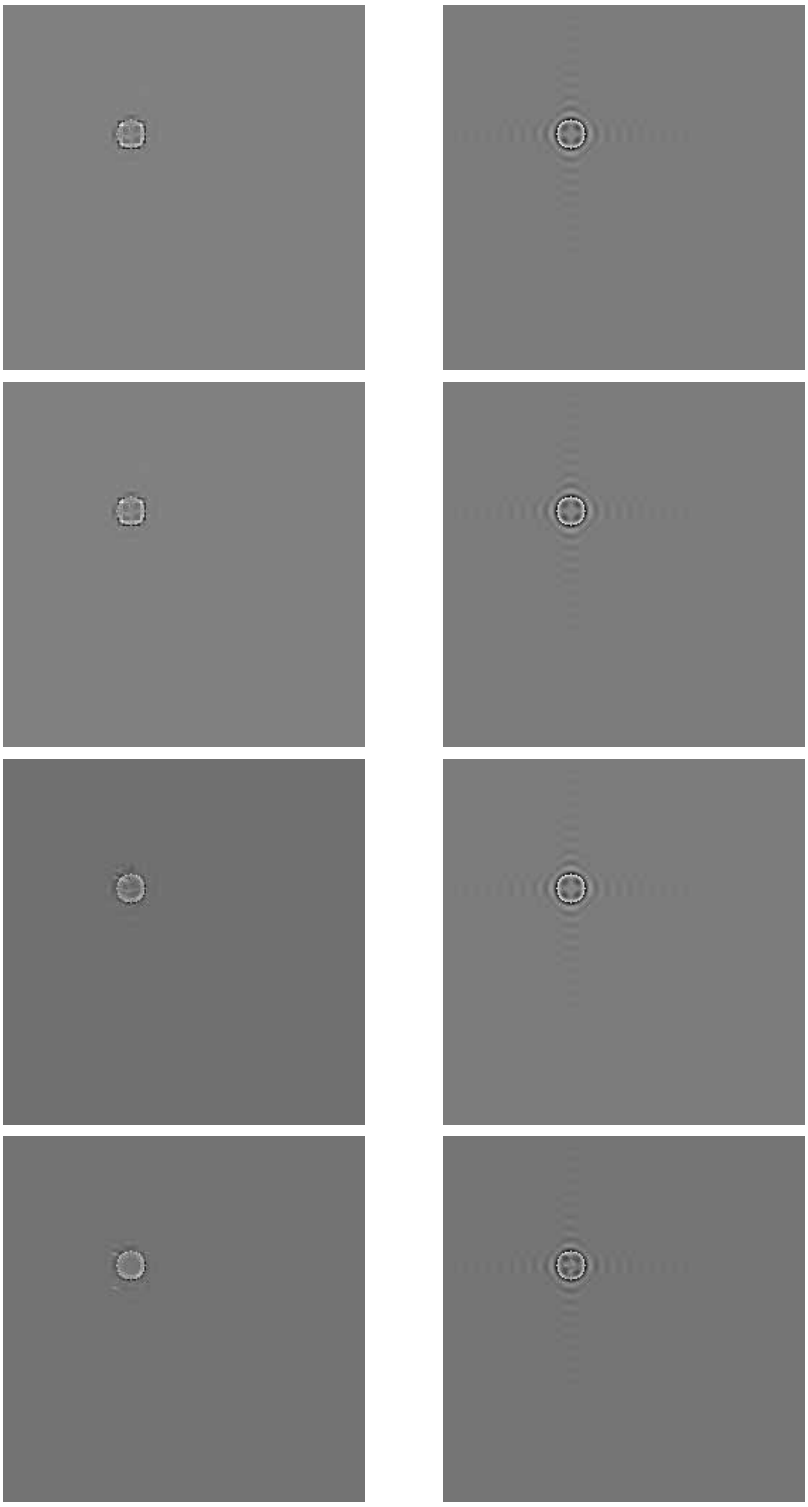

Figure 7: Left: Sequence of error images obtained using WT-based keyhole method. Right: Sequence of error images obtained using FT-based method.